Materials Science & Engineering A 706 (2017) 136–141

Contents lists available at ScienceDirect

Materials Science & Engineering A

journal homepage: www.elsevier.com/locate/msea

Impact toughness transition temperature of ferritic Fe-Al-V alloy with strengthening Fe_2AlV precipitates

P.A. Ferreirós[a,b], P.R. Alonso[a], G.R. Gomez[c], G.H. Rubiolo[a,d,*]

[a] Gerencia Materiales (GAEN) - Comisión Nacional de Energía Atómica (CNEA), Instituto Sabato - Universidad Nacional de San Martín (UNSAM), Av. Gral. Paz 1499, San Martín, Buenos Aires B1650KNA, Argentina
[b] Universidad Tecnológica Nacional, Facultad Regional General Pacheco (UTN-FRGP), Av. Hipólito Yrigoyen 288, B1617FRP Gral. Pacheco, Buenos Aires, Argentina
[c] Tenaris Siderca R & D, Materials Department, Dr. Jorge A. Simini 250, B2804MHA Campana, Buenos Aires, Argentina
[d] Consejo Nacional de Investigaciones Científicas y Técnicas (CONICET), Godoy Cruz 2290, C1425FQB Ciudad Autónoma de Buenos Aires, Argentina

ARTICLE INFO

Keywords:
Ferrous alloy
Fe_2AlV
Charpy test
High temperature
Brittle-to-ductile transition

ABSTRACT

The Fe_2AlV-strengthened ferritic alloys show an appreciable flow stress and creep strength up to 700 °C, comparable to those of other iron aluminide based alloys with coherent microstructures. In the present study, the brittle-to-ductile transition temperature (BDTT) of the $Fe_{76}Al_{12}V_{12}$ alloy was investigated in the peak hardness condition by Charpy test. A BDTT value of 617 °C was estimated using the criterion of the midpoint of the impact-energy transition region. An attempt is made to gain understanding of the micro-mechanisms controlling the fracture process and their interaction with the microstructure in order to identify ways for enhancing ductility in disordered Fe-Al alloys strengthened by coherent precipitates.

1. Introduction

The highest service temperature of current commercial ferritic steels in fossil-energy power plants is limited to ~ 600 °C due to the coarsening of the incoherent strengthening carbides [1]. In order to increase the steam temperatures and pressures, new advanced ferritic steels with better creep resistance are needed. Using the concept of precipitation strengthening, coherent B2-ordered NiAl-type precipitates have been investigated to reinforce α-iron for high-temperature applications [2–9]. These NiAl-strengthened ferritic alloys have typical chemical composition based on the pseudo-binary section Fe + 2.5 at% Al-NiAl + 1.25 at% Al with a maximum solvus temperature of 1000 °C that decreases with decreasing volume fraction of the B2 phase [3]. It has long been known that NiAl precipitates are responsible for increasing yield strength at moderate temperatures of an iron (bcc) solid-solution and to decrease it sharply between 600 and 700 °C [10]. The hardening mechanism below 550 °C was identified as the [111] slip shearing of NiAl precipitates, the sharp decrease in yield stress above 550 °C is not clearly understood because the NiAl precipitates dissolved into the matrix above 750 °C [11]. The B2 phase volume fraction, the average precipitate size and its coarsening resistance are factors affecting the creep properties of NiAl-strengthened ferritic alloys. Dislocation local climb over particles is the dominant strengthening mechanism for dislocation-precipitate interactions during creep in NiAl-strengthened ferritic alloys [2,3,12]. The threshold stress, i.e, the stress at which the secondary creep rate by dislocation climb goes to zero, is proportional to the Orowan stress and so it depends of precipitate-volume fraction and particle radius. In this way, the threshold stress decreases with increasing NiAl volume fraction but increases with increasing particle size. Then, for applications in fossil-energy power plants, a good creep resistance at operating stress and temperature could be obtained by choosing a suitable NiAl volume fraction and reducing the particle coarsening rate during long-term service. When the NiAl-strengthened ferritic alloy has been designed to meet all the mechanical properties above mentioned, the reported results of the four-point bending tests show that the brittle-to-ductile transition temperature (BDTT) is relatively high, i.e. between 400 and 500 °C [3]. The excessive aluminum content in the α matrix [13] together with the presence of hyperfine precipitates [4,5], the brittleness of NiAl at room and intermediate temperatures (< 400 °C) [7] and the coarse grain size (~ 100 μm [5]) are all factors that are believed to contribute to poor room and intermediate temperature ductility.

From the pioneering research of Zhao et al. [14] and Maebashi et al. [15] it is known that a miscibility gap also exists in the Fe-Al-V system between the disordered A2 and $L2_1$-ordered Fe_2AlV phases. This miscibility gap extend roughly in the composition range 5–25 at% Al and 0–25 at% V; it shrinks when the temperature increases up to 750 °C and then a two-phase equilibrium (B2-ordered Fe(Al,V) + $L2_1$) appears

* Correspondence to: Gerencia Materiales, Comisión Nacional de Energía Atómica, Av. Gral. Paz 1499, B1650KNA San Martin, Buenos Aires, Argentina.
E-mail address: rubiolo@cnea.gov.ar (G.H. Rubiolo).

http://dx.doi.org/10.1016/j.msea.2017.09.001
Received 27 April 2017; Received in revised form 28 August 2017; Accepted 2 September 2017
Available online 04 September 2017
0921-5093/

[16]. So, in fairly recent times, the research on Fe_2AlV-strengthened ferritic alloys has gained attention [16–18]. The $Fe_{1-2x}Al_xV_x$ alloys quenched from 1100 °C and aged at 700 °C/2 h show spherical precipitates of $L2_1$ phase for $X < 0.13$ and the hardness values, measured at room temperature, increases as the volume fraction of $L2_1$ phase precipitates does [16]. The dependence with temperature of compressive flow stress of a $Fe_{72}Al_{18}V_{10}$ alloy was shown to behave in a similar way as the NiAl-strengthened ferritic alloys, ie, a considerable higher yield strength than the $Fe_{82}Al_{18}$ solid solution at moderate temperatures and then, between 600 and 700 °C, a sharp decrease [17]. A classic precipitation hardening behavior has been observed along the time for aging treatments in the range 600–700 °C of the ferritic $Fe_{76}Al_{12}V_{12}$ alloy, it was shown that strength at room temperature is controlled by a precipitate shearing mechanism for sizes around that of peak strengthening (~ 10 nm) and the Orowan dislocation bypass mechanism for larger sizes [18]. Compressive creep tests have been performed for the two-phase alloys $Fe_{78}Al_{17}V_5$ and $Fe_{72}Al_{18}V_{10}$ between 650 and 750 °C, the stress dependence of secondary creep rate at each temperature resembles the theoretical modelling of the creep behavior of precipitation-strengthened materials as the case of NiAl-strengthened ferritic alloy [17]. As mentioned above, intermediate temperature ductility is an important property for ferritic steels used in fossil-power power plants, but this issue has not yet been investigated in Fe_2AlV-strengthened ferritic alloys.

This study has been planned to characterize for first time the BDTT of the Fe_2AlV-strengthened ferritic $Fe_{76}Al_{12}V_{12}$ alloy. This alloy was aged a 700 °C for a time period such that peak hardening at room temperature is reached. Impact toughness test were performed in the temperature interval from 450 to 700 °C using a novel device that heat the specimen by AC current while it stay in the specimen support of a Charpy test machine. From these results, we may get some new insight into the mechanisms responsible for deformation and ductility improvement of Fe_2AlV-strengthened ferritic alloys.

2. Experimental procedure

2.1. Materials and sample preparation

Alloy buttons of 30 g were melted in an electric arc furnace with tungsten electrode and water cooled copper crucible under argon atmosphere. The purity of the used components was 99.97% Fe, 99.99% Al and 99.7% V. The buttons were then heated in an electric furnace under argon atmosphere up to 1100 °C and hot rolled in several passes (10 or 12 times with von Mises strain $\varepsilon < 0.1$ for each step) to get a plate about 3 mm thick. Mechanical polish was used to reach a final plate thickness of 2.5 mm. The average chemical composition of one rolled button alloy was measured by electron-probe microanalysis in a Cameca SX50 equipment (Table 1). The composition values were obtained from the average and standard deviation of 50 measurement points along a straight line of 10 mm. Charpy-V notch samples for impact tests were prepared from the plates according with the sub-size specimen ASTM E23-07 recommendations [19]. One bar of 2.5 × 10 × 55 mm was machined by electro-discharge machining (EDM) from each hot rolled plate and all of them were orientated in longitudinal-transverse rolling direction. Afterwards, the bars were wrapped in a Tantalum foil and heat-treated at 900 °C for 30 min (A2 solution) and then at 700 °C for 22 min (A2 + $L2_1$ aging) into a quartz tube at vacuum atmosphere. Finally, by using EDM, a 45° V-notch was cut to a depth of 2 mm into each bar to obtain the impact toughness specimen.

A low purity ingot of the $Fe_{76}Al_{12}V_{12}$ alloy has been produced from the melt by casting under reducing atmosphere. The alloy components were melting in an alumina crucible by electric induction and pouring into a rectangular hybrid carbon steel/ceramic mold 40 mm thick, 60 mm width and 80 mm high. Commercial purity aluminum and mild steel wires (Ø 4 mm) and commercial ferro-vanadium (lumps of 10–50 mm) were used as raw materials. The ingot chemical composition (Table 1) was measured by Wavelength Dispersive X-ray Fluorescence on a Bruker S8 Tiger equipment. Cylindrical sample of 10 mm diameter and 15 mm height, for compression test, were cut from the ingot by EDM. The axis of the cylindrical sample is parallel to the thickness of the ingot and therefore parallel to the axis of the columnar grains. Prior to the compression test, the samples had a heat solution treatment and aging similar to the samples for Charpy tests.

For light optical microscopy the samples were ground (up to 600 grit), polished (5 μm diamond) and etched in acidic solution (68% glycerol, 16% HF and 16% HNO_3). The microstructure was observed by means of a Transmission Electron Microscope (TEM) (Philips CM200 operated at 160 kV). Thin foils for TEM were prepared by cutting 3 mm diameter and 500 μm thickness discs using EDM, mechanically grinding the discs to 100 μm thickness, and final electrolytic thinning of the discs using a double-jet electro polisher STRUERS Tenupol-5 with an electrolyte comprising 67% methanol and 33% nitric acid. Double tilt sample holder was used for TEM observation performed with the foil normal in the [011] direction and dark field image was took in the [11$\bar{1}$] direction.

2.2. Mechanical testing

Hot compressive tests were conducted on a Gleeble-3500 thermal simulation machine at temperatures of 600 and 650 °C at $\dot{\varepsilon} = 5 \times 10^{-4}\ s^{-1}$ constant strain rate.

The impact tests were perform in a Charpy Otto Wolpert-Werke PW 5 S5 (50 J) machine. The testing machine was equipped with a device for in-situ Joule heating of the specimen [20]. This heating method requires a control thermocouple located at 3 mm of notch section of the specimen and the previous knowledge of the sample temperature profile for several control temperatures (T_C) in the impact test range. Fig. 1a shows the temperature profiles measured in a $Fe_{76}Al_{12}V_{12}$ alloy dummy sample together with the fitting curves coming from a thermal model developed in reference [20]. The plastic zone in the fracture process is located approximately inside of a volume which extends from the notch section to a distance equal to the thickness of the specimen [21]. So, we take the confidence interval of temperature for the impact test as the difference of temperature inside of the mentioned volume. Fig. 1b shows the dependence of this confidence interval of temperature with the control temperature as derived from the results of Fig. 1a.

3. Results and discussion

The grains microstructure features of the aged Charpy and compression samples are shown in Fig. 2. Equiaxial grains with average size of 700 μm characterize the Charpy sample structure. Instead, the sample for the compression test shows columnar grains aligned in the direction of the cylinder axis. The aging treatment applied to both types of samples produces its maximum hardening at room temperature due to a microstructure of spherical coherent $L2_1$ (Fe_2AlV) precipitates,

Table 1
Measured composition (at%) on $Fe_{76}Al_{12}V_{12}$ alloys.

Alloy type	Fe	Al	V	C	Mn	Si	S (ppm)
Button	75.83 ± 0.18	11.89 ± 0.15	12.28 ± 0.13	–	–	–	–
Ingot	76.10 ± 0.27	11.01 ± 0.14	11.72 ± 0.06	0.252 ± 0.006	0.355 ± 0.007	0.525 ± 0.023	374 ± 34

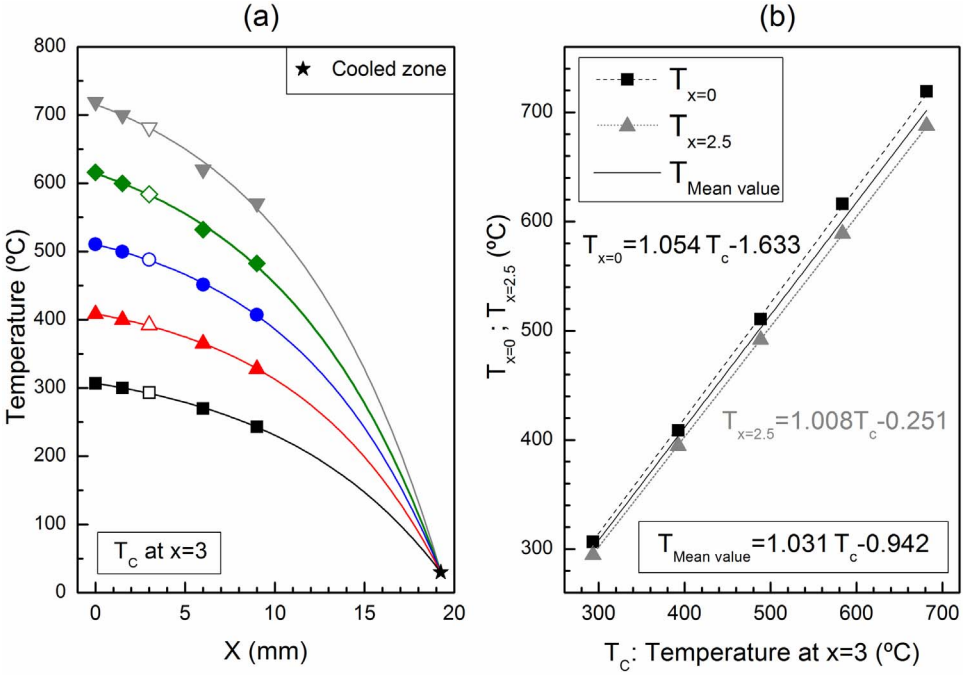

Fig. 1. Temperature calibration prior to Charpy tests. a) Temperature profiles of the V-notch Charpy impact sample heated by AC current. Open symbols represent the control thermocouple value (Tc). The symbols are measured values and the continuous lines come from calculations made with a thermal model (see text). b) Confidence interval for the temperature at the fracture process volume as function of the control temperature.

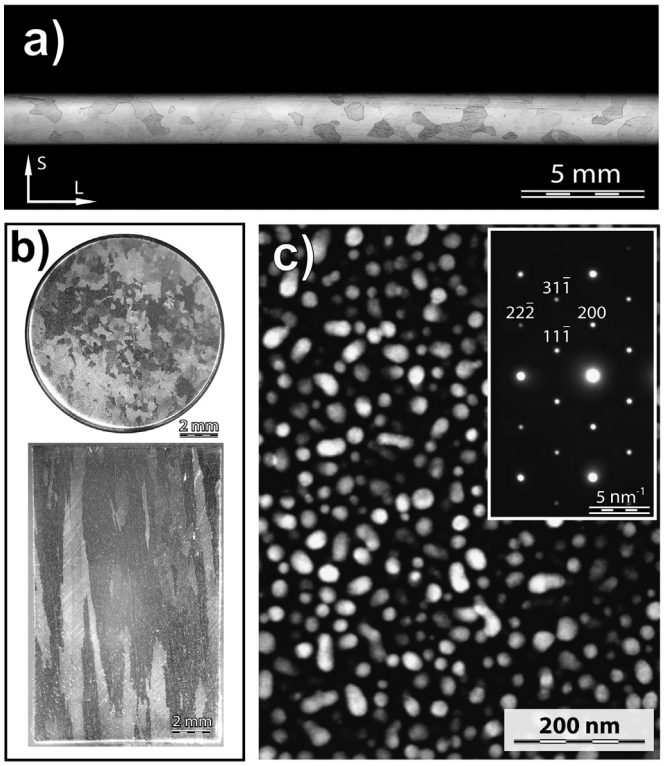

Fig. 2. The microstructures of $Fe_{76}Al_{12}V_{12}$ alloy samples aged at 700 °C for 22 min: (a) optical micrograph showing the average grain size of the Charpy sample. Specimen orientation is indicated by arrows (ASTM E23-07), (b) optical macrographs showing the columnar grain structure of the compression sample. (c) TEM dark field (DF) micrograph using $[11\bar{1}]$ $L2_1$ reflection showing the Fe_2AlV ($L2_1$) precipitates.

average diameter of 22 nm and volume fraction of 22% (see dark-field TEM image of precipitates in Fig. 2c), within an A2 matrix whose average chemical composition of aluminum plus vanadium is about 18 at% [18].

As the brittle ductile transition can be interpreted quantitatively as a result of the competition between the flow stress and the cleavage strength (also known as brittle fracture stress) of the material, then the knowledge of the flow stress temperature dependence is one of the most important aspects when discussing the temperature at which occurs the transition. The flow stress temperature dependence of the $Fe_{72}Al_{18}V_{10}$ alloy in as cast condition had been reported by Senčekova et al. [17], this alloy consist of an A2 matrix with coarse grains of 500 μm containing $L2_1$ precipitates with an average size of 30 nm. The volume fraction of precipitates was not reported but can be assumed close to that of the $Fe_{76}Al_{12}V_{12}$ alloy due to its nearby chemical compositions. Our results of the compressive flow stress of the $Fe_{76}Al_{12}V_{12}$ alloy in pre-aged 700 °C/22 min was measured at 600 °C and 650 °C are shown in Fig. 3 compared against those of the $Fe_{72}Al_{18}V_{10}$ alloy. As can be seen, the strength at 600 °C and 650 °C are similar in both alloys, this fact allow us to take the flow stress temperature dependence of the $Fe_{72}Al_{18}V_{10}$ alloy as a reference behavior for the flow stress of the $Fe_{76}Al_{12}V_{12}$ alloy in the wide range of test temperatures in which we investigated its ductility using the Charpy test. A proof that the $L2_1$ precipitates also affect the strength of the alloy at high temperature can be observed in Fig. 3 comparing against the flow stress of a solid solution $Fe_{83}Al_{17}$ alloy [13] with an aluminum content about the same than the (Al + V) content in the A2 matrix of the $Fe_{76}Al_{12}V_{12}$ alloy. This

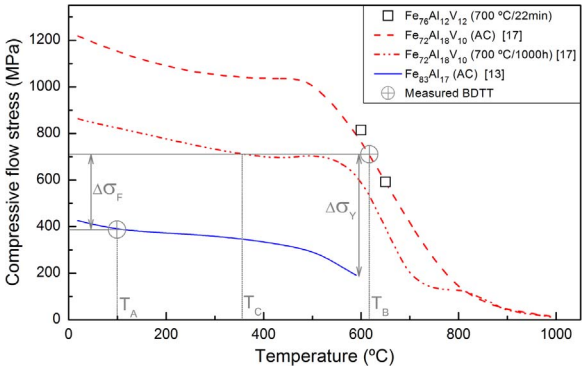

Fig. 3. The compressive flow stress at $\dot{\varepsilon} = 5\times10^{-4}s^{-1}$ of the $Fe_{76}Al_{12}V_{12}$ alloy in the condition aged at 700 °C for 22 min compared to that of the $Fe_{72}Al_{18}V_{10}$ alloy at $\dot{\varepsilon} = 1\times10^{-4}s^{-1}$ in the conditions as-cast and aged at 700 °C for 1000 h. The compressive flow stress of a solid solution Fe-Al alloy is given for comparison.

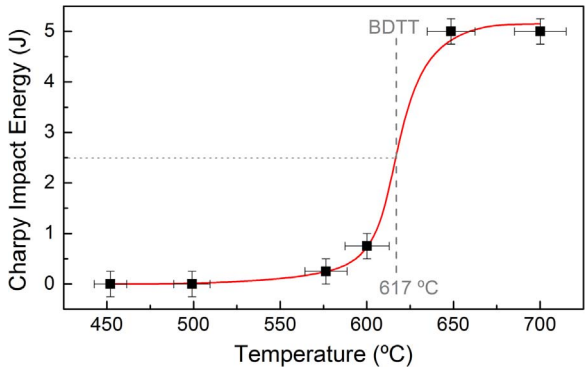

Fig. 4. Charpy transition curve of the $Fe_{76}Al_{12}V_{12}$ alloy in the condition aged at 700 °C for 22 min. The position of BDTT criterion is shown.

polycrystalline alloy had grain sizes of the order of 1 mm.

The results of the Charpy impact test are displayed in Fig. 4, where the dissipated energy is plotted against the test temperature. A clear impact-energy transition region is observed between 576 °C and 648 °C. The analysis of the fractured surfaces allows correlate this energy transition with a ductile to brittle fracture transition (Fig. 5). In the ductile zone (648 and 700 °C) the perimeter sections of test samples shows a high degree of deformation, instead the perimeter sections remain rectangular in the brittle zone (500 and 576 °C). In addition, the enlargements in the fractographs of Fig. 5 shows a trans-grain fracture with smooth and shiny surfaces (cleavage) for the brittle sample (576 °C) and a fracture with opaque and curved surfaces for ductile sample (648 °C). Finally, a BDTT value of 617 °C was estimated using the criterion of the midpoint of the impact-energy transition region [22].

The BDTT displayed by the $Fe_{76}Al_{12}V_{12}$ alloy, in the condition aged at 700 °C for 22 min, is a high value for its application in fossil-energy power plants. However, it compares well with the BDTT values of NiAl-strengthened ferritic alloys in the solution-treated and air-cooled condition where there is a homogeneous distribution of precipitates with a size of around 50 nm [3]. Also, it is far below the BDTT values of Fe-Al-Ti alloys with similar (A2 + $L2_1$) microstructure [23,24]. Therefore, this is a positive starting point for future research aimed at lowering of the BDTT of Fe_2AlV-strengthened ferritic alloys.

In order to identify ways for enhancing ductility in disordered Fe-Al alloys strengthened by coherent precipitates it is necessary to gain understanding of the micro-mechanisms controlling the fracture process and their interaction with the microstructure. The connection between the precipitation hardening and the BDTT can be phenomenological understood on the basis of a Yoffee-type diagram [25] as shown in Fig. 3. In reference [13] the toughness of the $Fe_{83}Al_{17}$ alloy was studied by Charpy impact testing using specimens of dimensions 3 × 4 × 27 mm^3 with notch according to German standard DIN EN 10045, therefore the crack tip stress in their test is comparable to ours and both scale in the same way with the flow stress. So, from the intersection of the measured BDTTs (T_A and T_B) with its respective flow stress curve it can be obtained the increase of the brittle fracture stress ($\Delta\sigma_F$) between both alloys. This analysis indicates that precipitation hardening also increases the fracture stress but the effect is less than over the flow stress ($\Delta\sigma_y$) and the result is that the BDTT increases. The rationale behind this is that the hardening mechanism in the $Fe_{76}Al_{12}V_{12}$ alloy at peak aged condition is the shearing of coherent particles by dislocations [18]. The moving dislocations shear the particles, these are destroyed, the slip plane weakens, and the slip occurs

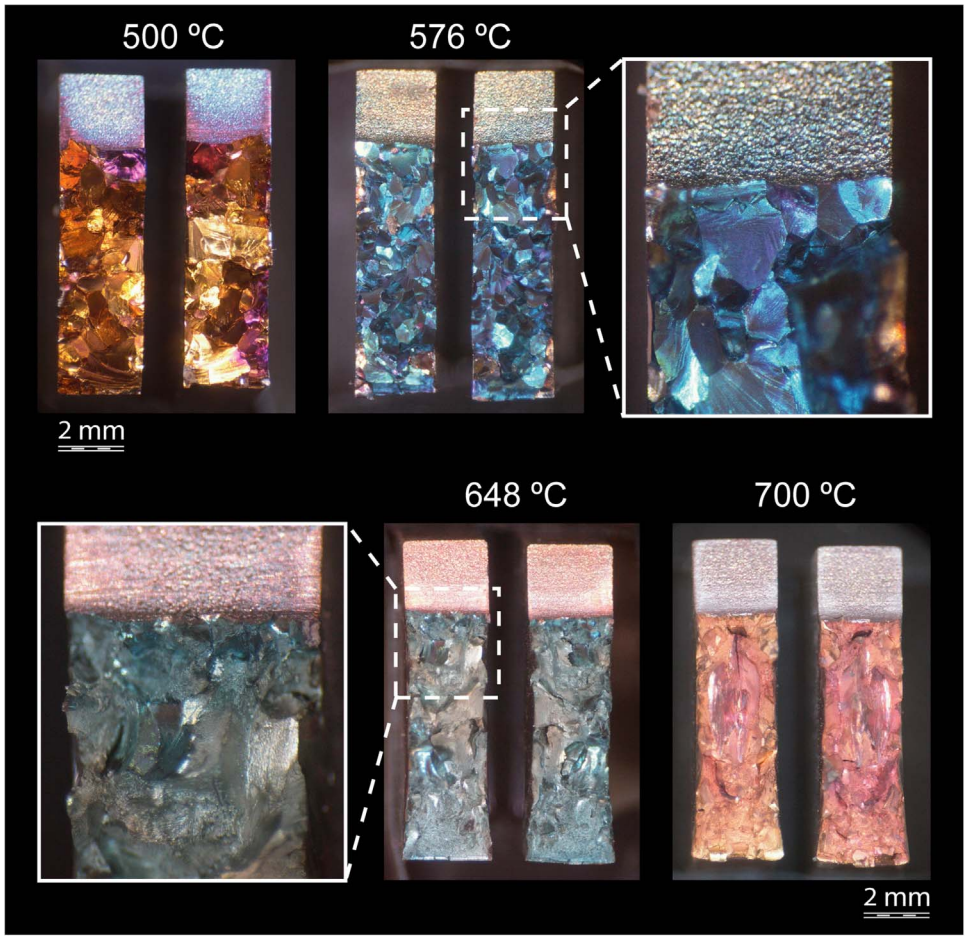

Fig. 5. Macrofractographs of the impacted samples. The upper and down sample rows correspond to the brittle and ductile fracture process, respectively. In the online article view, the different color of the fracture surfaces is due to the oxide formed at the different test temperatures. (For interpretation of the references to color in this figure legend, the reader is referred to the web version of this article).

preferentially on these planes. The dislocations form intense slip bands and pile up against grain boundaries which results in an inhomogeneous slip distribution [26]. The critical number of pile-up dislocations yielding to transgranular fracture is reached with a smaller deformation when it is concentrated in lesser number of sliding bands than if the slip was not so local. So, both the fracture deformation and, in consequence, the fracture stress decrease as the slip band width decreases [27,28]. As confirmed by experimental observations in, for example, precipitation hardened Al-Li-Cu [27] and Ti-Al [28] alloys; decreasing slip band width is accompanied by increasing flow stress. Moreover, the results also suggest that the slip band width has the opposite behavior to the flow stress with the aging time [27]. Thus, the present analysis suggests that strengthening by shear precipitates results in a greater increase in the flow stress than in the fracture stress due to the location of the deformation resulting from a local reduction of the resistance to the movement of dislocations which arises from the reduction of the cross-section of the precipitate by shearing.

In addition to the degree of particle hardening an influence of grain size on the fracture stress behavior has been observed for such an inhomogeneous slip distribution. Several investigations in precipitation hardened alloys of Fe-Ni-Al (γ-alloy) [29], Ti-Al-Si [30] and Ti-Al [28] systems have shown a drastic decrease of ductility and fracture stress with increasing grain size following a Hall-Petch type relationship.

The discussion in the last two paragraphs suggests that by careful control of grain size and precipitate's coherency, through its size, the alloy may be made that is both resistant to deformation and tough. For example, the prolonged heat treatment of the $Fe_{72}Al_{18}V_{10}$ alloy reduces the flow stress as shown in Fig. 3 due to the over-aging of the precipitates but, according to the proposed micro-mechanism controlling the fracture process, the deformation should become more homogeneous and the fracture stress should be greater or equal to its value for the size of precipitate in the peak-age condition. Then, following Yoffee's criteria, the BDTT (T_C) should be reduced considerably as shown in Fig. 3. This processing route has been employed in the NiAl-strengthened ferritic alloys, a two-step aging heat treatment (48 h at 900 °C followed by 300 h at 750 °C), which produces duplex precipitates sizes, shifted the BDTT value from 625 °C to 425 °C [3]. Recently, the improvement of ductility by reduction of grain size was tested in the Fe_2AlTi-strengthened ferritic alloy $Fe_{73}Al_{22}Ti_5$ built by melting powders layer by layer with a laser beam [31]. The samples with an average grain size of about 10 μm were ductile (> 3% bending in the outer fiber) at 500 °C while the as-cast reference samples with an average grain size of about 100 μm show only 2% bending in the outer fiber at 750 °C. Other thermomechanical routes that could produce recrystallization and grain refinement are hot extrusion, rolling or forging. An example in this sense is found in the $Fe_{73}Al_{25}Ta_2$ alloy (B2 matrix + $L2_1$ + C14 Laves phase) whose BDTT in the as-cast condition was measured at 750 °C [32] and after forging it was reduced to 525 °C [33]. Preliminary studies on the $Fe_{76}Al_{12}V_{12}$ alloy by changing the hot rolling parameters, ie the rate of deformation and the temperature within the A2 phase domain, have shown that its dynamic recrystallization with grain refinement is possible [34]. However, the forging should be better to obtain a homogeneous grain refinement in all the volume of the material. Following these routes further studies are being carried out to obtain the reduction in the DBTT of the alloy through the reduction of the grain size of the matrix A2 and the coarsening of the precipitate $L2_1$ holding a good resistance to the deformation at high temperature.

4. Conclusions

The mechanical behavior of the Fe_2AlV-strengthened ferritic $Fe_{76}Al_{12}V_{12}$ alloy was investigated with the focus on the compressive flow stress and impact toughness between 450 and 700 °C. The samples were pre-aged 700 °C/22 min in order to obtain the peak hardness condition at room temperature. Both, yield stress levels at high temperatures and BDTT, compare well with those of the NiAl-strengthened ferritic alloy already investigated. It is hoped that the forging of the alloy at temperatures within the A2 phase and a heat treatment of over aging will produce grain refinement and more homogeneous deformation leading to reduction of the brittle-ductile transition temperature together with enough high temperature strength.

Acknowledgments

The authors thank the heads of the research groups belonging to Gerencia Materiales CAC-CNEA, Mr. A. Iorio and Dr. P.B. Bozzano and technical staff by offering facilities for this research. PAF was supported by the CNEA (Argentina) professional fellowship program.

References

[1] H.K.D.H. Bhadeshia, Design of ferritic creep-resistant steels, ISIJ Int. 41 (2001) 626–640.
[2] S.M. Zhu, S.C. Tjong, J.K.L. Lai, Creep behavior of a β'(NiAl) precipitation strengthened ferritic Fe-Cr-Ni-Al alloy, Acta Mater. 46 (1998) 2969–2976.
[3] C. Stallybrass, A. Schneider, G. Sauthoff, The strengthening effect of (Ni,Fe)Al precipitates on the mechanical properties at high temperatures of ferritic Fe–Al–Ni–Cr alloys, Intermetallics 13 (2005) 1263–1268.
[4] Z.K. Teng, C.T. Liu, G. Ghosh, P.K. Liaw, M.E. Fine, Effects of Al on the microstructure and ductility of NiAl-strengthened ferritic steels at room temperature, Intermetallics 18 (2010) 1437–1443.
[5] Z.K. Teng, C.T. Liu, M.K. Miller, G. Ghosh, E.A. Kenik, S. Huang, P.K. Liaw, Room temperature ductility of NiAl-strengthened ferritic steels: effects of precipitate microstructure, Mater. Sci. Eng. A 541 (2012) 22–27.
[6] Z.K. Teng, F. Zhang, M.K. Miller, C.T. Liu, S. Huang, Y.T. Chou, R.H. Tien, Y.A. Chang, P.K. Liaw, New NiAl-strengthened ferritic steels with balanced creep resistance and ductility designed by coupling thermodynamic calculations with focused experiments, Intermetallics 29 (2012) 110–115.
[7] Z. Sun, C.H. Liebscher, S. Huang, Z. Teng, G. Song, G. Wang, M. Asta, M. Rawlings, M.E. Fine, P.K. Liaw, New design aspects of creep-resistant NiAl-strengthened ferritic alloys, Scr. Mater. 68 (2013) 384–388.
[8] Z.B. Jiao, J.H. Luan, Z.W. Zhang, M.K. Miller, C.T. Liu, High-strength steels hardened mainly by nanoscale NiAl precipitates, Scr. Mater. 87 (2014) 45–48.
[9] Z. Sun, G. Song, J. Ilavsky, P.K. Liaw, Duplex precipitates and their effects on the room-temperature fracture behaviour of a NiAl-strengthened ferritic alloy, Mater. Res. Lett. 3 (2015) 128–134.
[10] C. Stallybrass, G. Sauthoff, Ferritic Fe–Al–Ni–Cr alloys with coherent precipitates for high-temperature applications, Mater. Sci. Eng. A 387–389 (2004) 985–990.
[11] T. Edahiro, K. Kouzai, H.Y. Yasuda, Mechanical properties and hardening mechanism of Fe–Al–Ni single crystals containing NiAl precipitates, Acta Mater. 61 (2013) 1716–1725.
[12] S. Huang, D.W. Brown, B. Clausen, Z. Teng, Y. Gao, P.K. Liaw, Metall. Mater. Trans. A 43 (2012) 1497–1508.
[13] J. Herrmann, G. Inden, G. Sauthoff, Deformation behaviour of iron-rich iron-aluminium alloys at high temperatures, Acta Mater. 51 (2003) 3233–3242.
[14] P.Z. Zhao, T. Kozakai, T. Miyazaki, Phase separations into A2 + DO3 two phases in Fe-Al-V ternary ordering alloys, J. Jpn. Inst. Met. 53 (1989) 266–272.
[15] T. Maebashi, T. Kozakai, M. Doi, Phase equilibria in iron-rich Fe-Al-V ternary alloy system, Z. Met. 95 (2004) 1005–1010.
[16] P.A. Ferreirós, P.R. Alonso, P.H. Gargano, P.B. Bozzano, H.E. Troiani, A. Baruj, G.H. Rubiolo, Characterization of microstructures and age hardening of Fe1-2xAlxVx Alloys, Intermetallics 50 (2014) 65–78.
[17] L. Senčekova, M. Palm, J. Pešička, J. Veselý, Microstructures, mechanical properties and oxidation behaviour of single-phase Fe3Al (D03) and two-phase α-Fe,Al (A2) + Fe3Al (D03) Fe-Al-V alloys, Intermetallics 73 (2016) 58–66.
[18] P.A. Ferreirós, P.R. Alonso, G.H. Rubiolo, Coarsening process and precipitation hardening in Fe2AlV-strengthened ferritic Fe76Al12V12 alloy, Mater. Sci. Eng. A 684 (2017) 394–405.
[19] ASTM Standard E23-07a, Standard Test Methods for Notched Bar Impact Testing of Metallic Materials, ASTM, West Conshohocken, PA, 2007, pp. 1–28.
[20] P.A. Ferreirós, P.R. Alonso, P.H. Gargano, G.H. Rubiolo, High-temperature testing in a Charpy impact pendulum using in-situ Joule heating of the specimen, submitted to Fatigue Fract, Eng. Mater. Struct. (2017).
[21] M.P. Manahan, R.B. Stonesifer, Y. Soong, J.M. Burger, Miniaturized notch test specimen and test machine design, in: T.A. Siewert, K. Schmieder (Eds.), Pendulum Impact Machines: Procedures and Specimens for Verification, ASTM STP 1248, American Society for Testing and Materials, West Conshohocken, PA, 1995, pp. 39–69.
[22] R. Viswanathan, Damage Mechanisms and Life Assessment of High-temperature Components, 44073 ASM International, Metals Park, Ohio, 1993, pp. 21–45.
[23] R. Krein, M. Palm, M. Heilmaier, Characterization of microstructures, mechanical properties, and oxidation behavior of coherent A2 + L21 Fe–Al–Ti, J. Mater. Res. 24 (2009) 3412–3421.
[24] R. Krein, M. Friak, J. Neugebauer, M. Palm, M. Heilmaier, L21-ordered Fe–Al–Ti

alloys, Intermetallics 18 (2010) 1360–1364.
[25] R.W. Armstrong, Material grain size and crack size influences on cleavage fracturing, Philos. Trans. R. Soc. A 373 (2015) 20140124.
[26] E. Hornbogen, E.A. Starke Jr, Theory assisted design of high strength low alloy aluminum, Acta Metal. Mater. 41 (1993) 1–16.
[27] K.V. Jata, E.A. Starke Jr., Fatigue crack growth and fracture toughness behavior of an AI-Li-Cu alloy, Metall. Trans. A 17 (1986) 1011–1026.
[28] G. Terlinde, G. Luetjering, Influence of grain size and age-hardening on dislocation pile-ups and tensile fracture for a Ti-AI alloy, Metall. Trans. A 13 (1982) 1283–1292.
[29] K.H. Zum Gahr, L.J. Eberhartinger, The influence of grain diameter on the mechanical properties of a precipitation-hardenable austenitic steel, Z. Met. 67 (1976) 640–645.
[30] M.G. Mendiratta, S.M.L. Sastry, J.V. Smith, Effect of grain size upon flow and fracture in a precipitation-strengthened Ti-8 wt% Al-0.25 wt% Si alloy, J. Mater. Sci. 11 (1976) 1835–1842.
[31] A. Michalcová, L. Senčekova, G. Rolink, A. Weisheit, J. Pešička, M. Stobik, M. Palm, Laser additive manufacturing of iron aluminides strengthened by ordering, borides or coherent Heusler phase, Mater. Des. 116 (2017) 481–494.
[32] D.D. Risanti, G. Sauthoff, Strengthening of iron aluminide alloys by atomic ordering and Laves phase precipitation for high-temperature applications, Intermetallics 13 (2005) 1313–1321.
[33] P. Hanus, E. Bartsch, M. Palm, R. Krein, K. Bauer-Partenheimer, P. Janschek, Mechanical properties of a forged Fe–25Al–2Ta steam turbine blade, Intermetallics 18 (2010) 1379–1384.
[34] A.A. Becerra, P.A. Ferreirós, G.H. Rubiolo, Proceedings of the 15th International Congress of Science and Technology of Metallurgy and Materials CONAMET/SAM, Santiago, Chile, T04 ID:116, 2015.